10-9-2012

Plasmon Waveguide Resonance Raman Spectroscopy

Kristopher J. McKee
Iowa State University

Matthew W. Meyer
Iowa State University

Emily A. Smith
Iowa State University, esmith1@iastate.edu

Plasmon Waveguide Resonance Raman Spectroscopy

Abstract
Raman spectra were collected from a 1.25 M aqueous pyridine solution, 100-nm polystyrene film or a trimethyl(phenyl)silane monolayer at a plasmon waveguide interface under total internal reflection (TIR). The plasmon waveguide resonance (PWR) interface consisted of a sapphire prism/49 to 50 nm Au/548 to 630 nm SiO2 and a monolayer, thin film or aqueous analyte. The Raman peak area as a function of incident angle was measured using a 785-nm excitation wavelength, and was compared to the Raman peak area obtained at a sapphire or sapphire/50 nm Au interface. In contrast to measurements at a bare sapphire prism, increased surface sensitivity and signal were obtained from the PWR interface. In contrast to measurements at a bare Au film where only p-polarized incident light generates an enhanced interfacial electric field, plasmon waveguide interfaces enable excitation with orthogonal polarizations using s- or p-polarized incident light. The Raman scatter from a monolayer was recorded at the PWR interface with a signal-to-noise ratio of 5.6 when averaging 3 accumulations with 3 min acquisition times using nonresonant excitation, whereas no signal was recorded from a monolayer at the sapphire interface. The reflected light from the interface enabled the identification of the incident angle where the maximum Raman scatter was produced, and the Raman signal generated at the plasmon waveguide interface was modeled by the enhanced interfacial mean square electric field relative to the incident field. In comparison to the techniques on which this work was based (i.e., PWR spectroscopy, TIR Raman spectroscopy at the prism interface, and surface plasmon resonance (SPR) Raman spectroscopy at the prism/Au interface), chemical specificity was added to PWR spectroscopy, a signal enhancement mechanism was introduced for TIR Raman spectroscopy, and polarization control of the interfacial electric field was added to SPR Raman spectroscopy.

Disciplines
Chemistry | Inorganic Chemistry | Materials Chemistry | Organic Chemistry | Other Chemistry | Physical Chemistry

Comments
Reprinted (adapted) with permission from *Analytical Chemistry,* 84(21); 9049-9055. Doi: 10.1021/ac3013972.

analytical chemistry

Article

pubs.acs.org/ac

Plasmon Waveguide Resonance Raman Spectroscopy

Kristopher J. McKee, Matthew W. Meyer, and Emily A. Smith*

Ames Laboratory, U.S. Department of Energy, Ames, Iowa 50011-3111, United States
Department of Chemistry, Iowa State University, Ames, Iowa 50011-3111, United States

ABSTRACT: Raman spectra were collected from a 1.25 M aqueous pyridine solution, 100-nm polystyrene film or a trimethyl(phenyl)silane monolayer at a plasmon waveguide interface under total internal reflection (TIR). The plasmon waveguide resonance (PWR) interface consisted of a sapphire prism/49 to 50 nm Au/548 to 630 nm SiO_2 and a monolayer, thin film or aqueous analyte. The Raman peak area as a function of incident angle was measured using a 785-nm excitation wavelength, and was compared to the Raman peak area obtained at a sapphire or sapphire/50 nm Au interface. In contrast to measurements at a bare sapphire prism, increased surface sensitivity and signal were obtained from the PWR interface. In contrast to measurements at a bare Au film where only p-polarized incident light generates an enhanced interfacial electric field, plasmon waveguide interfaces enable excitation with orthogonal polarizations using s- or p-polarized incident light. The Raman scatter from a monolayer was recorded at the PWR interface with a signal-to-noise ratio of 5.6 when averaging 3 accumulations with 3 min acquisition times using nonresonant excitation, whereas no signal was recorded from a monolayer at the sapphire interface. The reflected light from the interface enabled the identification of the incident angle where the maximum Raman scatter was produced, and the Raman signal generated at the plasmon waveguide interface was modeled by the enhanced interfacial mean square electric field relative to the incident field. In comparison to the techniques on which this work was based (i.e., PWR spectroscopy, TIR Raman spectroscopy at the prism interface, and surface plasmon resonance (SPR) Raman spectroscopy at the prism/Au interface), chemical specificity was added to PWR spectroscopy, a signal enhancement mechanism was introduced for TIR Raman spectroscopy, and polarization control of the interfacial electric field was added to SPR Raman spectroscopy.

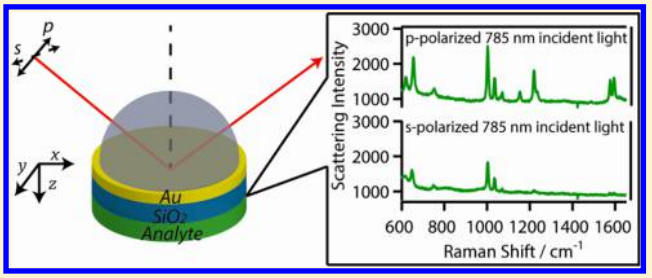

Total internal reflection (TIR) Raman spectroscopy measures chemically specific information from an analyte located within a hundred nanometers to a few micrometers from an interface.[1−10] Under TIR, the illuminating laser light is directed onto a prism/analyte interface at an incident angle higher than the critical angle (Figure 1a). Under these conditions, the Raman signal is confined to the interface as a result of the generated evanescent wave's limited penetration into the sample. Recently, the technique has seen increased use as modern technology has improved signal-to-noise ratios in TIR Raman spectra. The most current studies have focused on the behavior of adsorbates at various substrates and thickness measurements in polymer films.[11−15]

With approximately 1W visible excitation, TIR Raman scatter has been measured from a monolayer of zinc arachidate in 5 to 15 min.[11] Despite the benefit for many analytes of reduced spectral background using near IR excitation, acquiring TIR Raman signal from a monolayer or thin films is a challenge, largely due to the frequency dependence of Raman scatter.[16,17] The use of a thin Au film at the sample interface (Figure 1b) has been shown to enhance the Raman scatter, increase measurement reproducibility, and reduce background in TIR Raman spectroscopy.[18,19] Inclusion of the Au film increases the interfacial mean square electric field relative to the incident field (MSEF) and the generated Raman scatter at incident angles where surface plasmons are excited in the metal film. A 50-nm Au film, aqueous analyte and 785 nm excitation produces a 25-fold enhancement in the MSEF compared to an interface without the Au film. While Raman signal enhancement is expected at the Au interface, only p-polarized incident light excites surface plasmons in the Au film. This results in a MSEF enhancement primarily in the z-direction and to a minor extent in the x-direction (Figure 1). No increase in the MSEF is generated at the Au interface with s-polarized excitation, and information regarding the orientation and structure of the analyte layer may not be measured.

Plasmon waveguides reduce the full width half-maximum of the reflectivity curves and increase precision over traditional SPR spectroscopy.[20] The technique was coined plasmon waveguide resonance (PWR) spectroscopy. The most prolific use of PWR spectroscopy has been studies of cell membrane phenomena.[20−24] In the simplest case, a plasmon waveguide consists of a thin surface plasmon supporting metal film coated with a dielectric layer with a thickness of approximately $\lambda/2\eta$ or greater, where λ is the excitation wavelength and η is the dielectric material's refractive index (Figure 1c).[25,26] Plasmon

Received: May 22, 2012
Accepted: October 9, 2012
Published: October 9, 2012

   dx.doi.org/10.1021/ac3013972 | *Anal. Chem.* 2012, 84, 9049−9055

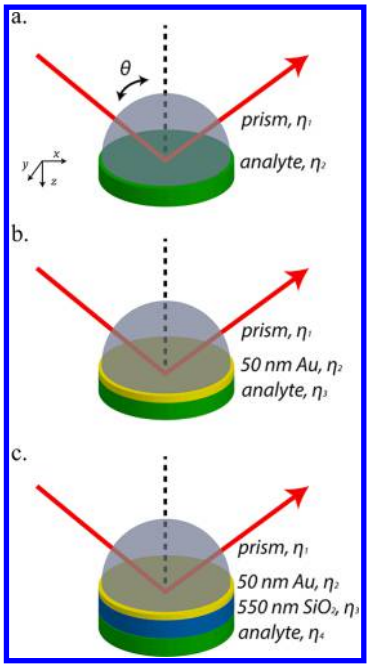

Figure 1. Experimental sample configuration for (a) total internal reflection (TIR) Raman spectroscopy, (b) surface plasmon resonance (SPR) Raman spectroscopy, or (c) plasmon waveguide resonance (PWR) Raman spectroscopy. The axes represents the orientation referred to throughout the text where the *z*-axis is perpendicular to the interface. In all experiments, η_1 is a sapphire prism.

waveguides operate by coupling surface plasmon modes in the metal to guided modes within the waveguide. The incident electric field is amplified at the dielectric interface and an evanescent wave is generated in the adjacent medium. The plasmon waveguide substrate enables both p- and s-polarized incident light to generate guided modes in the waveguide and produce enhanced interfacial electric fields oriented in the *x*-, *y*-, and *z*-directions.

In theory, plasmon waveguide substrates enable the characterization of TIR Raman scatter using orthogonal excitation polarizations, and increase the amount of Raman scatter generated at the interface. The purpose of this study is to quantify and model the generated Raman scatter at the plasmon waveguide interface and to compare this to the Raman scatter generated at the prism or prism/Au interface. Raman scatter from an aqueous 1.25 M pyridine solution, 100-nm polystyrene film, or trimethyl(phenyl)silane monolayer have been collected. The Raman signal generated at the plasmon waveguide interface has been modeled by calculations of the MSEF as a function of the incident angle and distance from the silica interface.

MATERIALS AND METHODS

Sample Preparation. Films were prepared on 25.4 mm sapphire disks (Meller Optics, Providence, RI). For the SPR and PWR films, 2 nm Ti was deposited as an adhesion layer followed by 49 ± 1 nm of Au (deposition performed by GWC Technologies Inc., Madison, WI). The PWR films were subsequently coated with 548 ± 2 nm of SiO_2 (performed by University of Minnesota Nanofabrication Center, Minneapolis, MN). Alternatively, 3 nm Ti followed by 50 ± 1 nm of Au were subsequently coated with 630 ± 4 nm of SiO_2 at Oak Ridge National Lab Center for Nanophase Materials Science. Film thicknesses were confirmed using a F20 series film measurement system (Filmetrics, San Diego, CA) operated in transmission mode for SiO_2 or reflection mode for Au. Prior to use, the substrates were cleaned in ethanol and dried with a stream of N_2 gas. A 2% polystyrene (Sigma-Aldrich, St. Louis, MO) solution was prepared in toluene (Fisher Scientific, Waltham, MA) and polystyrene films were then prepared by spin coating 200 μL of the polystyrene solution on a bare sapphire disk or a silica plasmon waveguide substrate at 3000 rpm for 1 min using a KW-4A spin coater (Chemat Technology, Inc. Northridge, CA).[27] The silane monolayer was formed from a 10% (v/v) trimethyl(phenyl)silane (Sigma Aldrich, 99% purity) solution prepared in N_2 purged toluene (60 min) by floating the substrate on the silane solution for 60 min. The substrate was rinsed copiously with toluene and water. Finally the substrate was dried with nitrogen, rinsed with isopropanol and again dried with nitrogen. A 1.25 M pyridine solution (Fisher Scientific, Waltham MA) was prepared in deionized water from an Easy Pure II purification system.

Raman Measurements. A previously described scanning angle TIR Raman microscope with 0.05° incident angle resolution was used to collect Raman and reflectivity spectra with 200 mW of 785 nm light incident at the sample.[18] The Raman scatter was collected on the analyte-side of the interface (Figure 1) using a 10× magnification, 0.30 NA microscope objective and a sapphire prism was used for all measurements. The polarization of the incident light was controlled by rotation of a half-wave plate in the optical path to deliver s- or p-polarized laser light at the sample interface. Measurements of the polarization at the sample indicated that less than 1% of the opposite polarization was present. Raman spectra and reflectivity measurements were acquired simultaneously in 1 min acquisitions for the pyridine and polystyrene samples and 3 accumulations with a 3 min acquisition time for the silane monolayer. Replicate measurements were obtained from consecutive scans through the incident angle range.

Data Analysis. Peak areas and intensities for the measured Raman modes were calculated by fitting them to Gaussian curves with the "Multipeak fitting 2" algorithm in IGOR Pro 6. The reflected light intensity and MSEF at the interface were calculated using 3-D finite-difference-time-domain (FDTD) based simulations (EM Explorer, San Francisco, CA) with a Yee cell size of 5 (Figure 2) or 1 (Figure 4) nm, 1000 cycles, and 0.1 to 0.01 (the latter was used close to the PWR angle, the former for all other angles) degree angle resolution. The calculations assumed all layers had a constant index of refraction and were homogeneous. The calculated reflectivity and MSEF curves account for the anisotropy of the sapphire prism.[28,29] The indices of refraction were: 1.762 (sapphire, p-polarization), 1.759 (sapphire, s-polarization), 0.143 + 4.799*i* (gold), 1.454 (silica), 1.578 (polystyrene, a good fit was obtained using this value for both p- and s-polarized excitation), and 1.347 (10% v/v pyridine in water).

RESULTS AND DISCUSSION

TIR, SPR, and PWR Interfaces. The goal of this work is to experimentally measure and model the Raman signals at a plasmon waveguide interface where MSEF enhancements are predicted when compared to an interface without the plasmon waveguide. Figure 1 illustrates the three interfaces studied in this work: (a) represents total internal reflection (TIR) Raman spectroscopy at the prism interface, (b) represents surface plasmon resonance (SPR) Raman spectroscopy at a Au

dx.doi.org/10.1021/ac3013972 | *Anal. Chem.* 2012, 84, 9049−9055

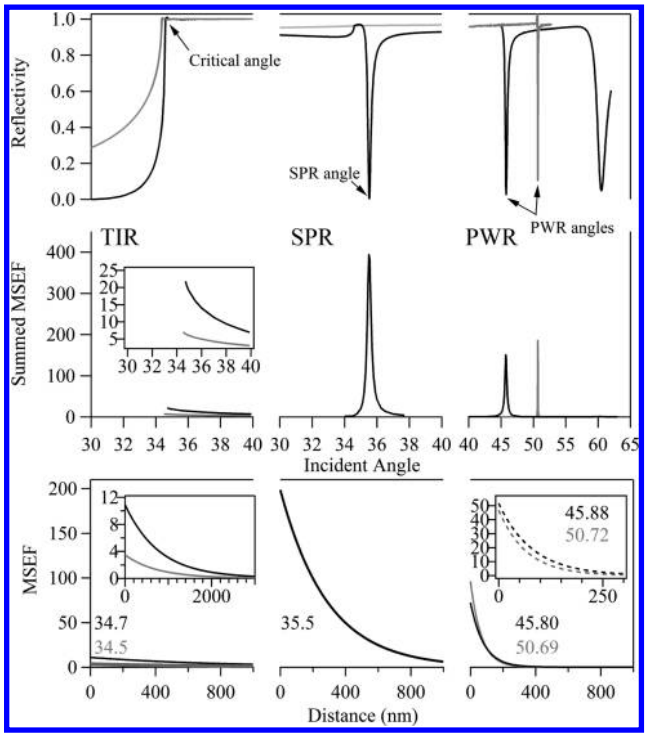

Figure 2. Calculated intensity of light reflected from the interface (top row); mean square electric field relative to the incident field summed from the interface to 5 nm away from the interface, where the Yee cell size for the calculations was 5 nm (middle row); and mean square electric field as a function of distance from the interface at the indicated angle (bottom row) for (left column) sapphire/air (TIR) interface; (middle column) 50 nm Au/air (SPR) interface; or (right column) 50 nm Au/630 nm SiO_2 plasmon waveguide/air (PWR) interface and p- (black) or s- (gray) polarized 785-nm incident light. An expanded view of the curves generated for the TIR interface are shown in the left insets and the curves corresponding to the experimental data shown in Figure 6 are shown in the right inset.

interface, and (c) represents plasmon waveguide resonance (PWR) Raman spectroscopy at a Au/SiO_2 interface. Calculated reflectivity and MSEF curves for the TIR, SPR, and PWR configurations are shown in Figure 2 for a 1.00 index of refraction "analyte" layer with 785 nm excitation. This interface closely approximates the measurement of a monolayer at a semi-infinite air interface. Reflectivity spectra predict the incident angle where the maximum Raman scatter for a given interface should be generated. In the TIR case, the critical angle is 34.4° (s-polarized excitation) or 34.6° (p-polarized excitation), corresponding to the largest interfacial MSEF. Near the critical angle the electric field extends approximately two micrometers from the interface. At an SPR interface, the highest interfacial MSEF is generated at the incident angle where the reflected light is maximally attenuated (i.e., the SPR angle, 35.5°) and surface plasmons are excited in the metal. Compared to the interface without the metal film, the SPR interface shows slightly better surface sensitivity since the MSEF does not extend as far away from the interface, and the MSEF at the interface (i.e., at the distance equal to zero in Figure 2) is 18 to 56× larger.

The reflectivity from the 50 nm Au/630 nm SiO_2 plasmon waveguide shows two minima for p-polarized incident light (45.75° and 60.50°) and a single minimum for s-polarized incident light (50.69°). The 45.75° and 50.69° minima correspond to the generation of waveguide modes that amplify the interfacial MSEF and are predicted to be the angles where the highest amount of Raman scatter is generated. Comparing the SPR and 630-nm silica PWR interfaces, a 39 to 48% lower MSEF is calculated at the PWR interface. On the other hand, the main benefit of PWR Raman spectroscopy over SPR Raman measurements is the ability to use both p- and s-polarized excitation. The 630-nm silica layer was chosen for these calculations because it matched the thickness used for the experimental measurements of a monolayer; different silica thicknesses significantly alter the PWR reflectivity and MSEF curves.

TIR, SPR, and PWR Raman Spectroscopy of a Homogeneous Solution. The plasmon waveguide interfaces used in this study had an optimal dielectric thickness for thin film measurements; however, it is useful to first measure the signal from a semi-infinite homogeneous solution where issues of analyte structure and orientation will not complicate data analysis. Raman spectra from a 1.25 M aqueous pyridine solution are shown in Figure 3 at TIR (a), SPR (b), and 550-

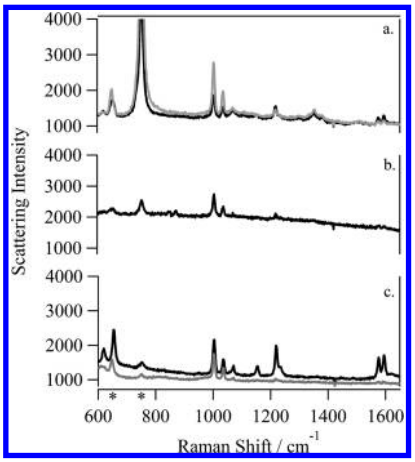

Figure 3. Raman spectra of 10% (v/v) pyridine at a (a) sapphire (TIR) interface, (b) 49 ± 1 nm Au (SPR) interface, or (c) 49 ± 1 nm Au/548 ± 2 nm SiO_2 plasmon waveguide (PWR) interface and p- (black) or s- (gray) polarized 785 nm incident light. The spectra were collected at TIR 50.00°, SPR 52.90°, or PWR p-polarization 49.85°, s-polarization 51.58°. These are the angles where the largest Raman scatter is collected at each interface. The discrepancy between the experimental and calculated critical, SPR, or PWR angle is within 0.25°. The asterisks (*) represent peaks that originate from the sapphire prism.

nm silica PWR (c) interfaces. The Raman spectra represent the incident angle where the highest signal was generated at each interface, and agree closely with calculated values of the critical angle, SPR angle, and PWR angles.

It appears from the data in Figure 3 that the TIR interface produces similar or more Raman scatter than the SPR or PWR interfaces, but additional factors must be considered. The extension of the MSEF from the interface is quite different for each interface and also depends on the polarization of the incident light (Figure 4). The further the MSEF extends from the interface, the more pyridine molecules are probed, which affects the amount of Raman scatter produced at each interface. Integrating the MSEF over the semi-infinite pyridine layer (Figure 4b), and considering each excitation polarization independently, the expected intensity of Raman scatter follows the order: PWR ≫ SPR > TIR (p-polarization) and PWR ≫ TIR (s-polarization). P- and s-polarized excitation will be

dx.doi.org/10.1021/ac3013972 | Anal. Chem. 2012, 84, 9049−9055

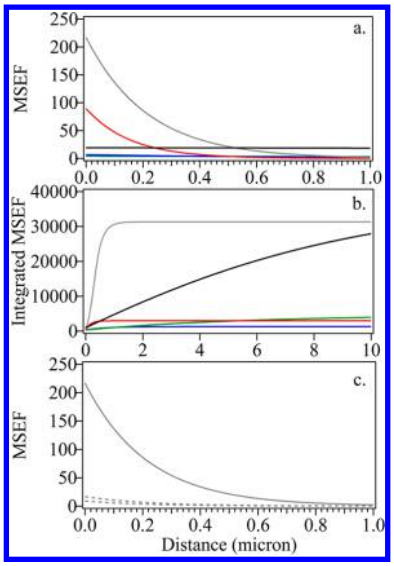

Figure 4. 3-D finite-difference-time-domain calculations of the mean square electric field (MSEF) as a function of the distance into a semi-infinite 10% (v/v) aqueous pyridine analyte layer and 550-nm silica PWR, SPR or TIR interfaces (gray, PWR s-polarized excitation at 51.58°), (black, PWR p-polarized excitation at 49.85°), (red, SPR p-polarized excitation at 52.90 degrees), (green, TIR s-polarized excitation at 50.0°), (blue, TIR p-polarized excitation at 50.0°). The same curves are shown in (b) after integration. (c) Calculations for the PWR interface using s-polarized excitation at the following incident angles: (solid) 51.58°, (dashed) 51.53°, and 51.63°.

considered independently since the depolarization ratio of each peak must also be considered, as further discussed below. For the 1003 cm^{-1} peak, the experimental Raman scatter follows the expected trend using p-polarized excitation, but the TIR interface produces more Raman scatter than the PWR interface using s-polarized excitation (Table 1). This deviation can be understood by considering the width of the PWR peak generated using s-polarized excitation is as narrow and the instrument's incident angle resolution of 0.05°. Figure 4c shows that a ± 0.05 incident angle uncertainty can significantly alter the amount of Raman scatter that is generated at the PWR interface using s-polarized excitation. There is also a spread in the incident angle, which is a result of the excitation beam being focused within the prism, and this is predicted to further decrease the amount of Raman scatter collected, particularly for the spectrum obtained at the PWR interface with s-polarized light. Uncertainties in the thickness of the Au or silica layers, as well as the accuracy of the measured indices of refraction will also generate differences between the calculated and experimental values at the SPR and PWR interfaces, but are not expected to be the main cause for the observed deviation.

Spectral background from the TIR prism is the main source of background in near IR-excitation TIR Raman spectroscopy. Previously, a reduction in the prism background was reported using a 50-nm Au film between the sapphire and analyte layer because of the limited transparency of the Au film.[30] A reduction in the prism background is also expected at the plasmon waveguide interface. On the other hand, several hundred nanometers of silica may contribute to the spectral background since the electric field intensity is high in the waveguide supporting medium (i.e., SiO_2). Comparing the sapphire peak intensity in Figure 3, there is a 11-fold or 58-fold reduction in the 750 cm^{-1} sapphire peak in the PWR spectrum compared to the TIR Raman spectrum using p- or s-polarized incident light, respectively. For s-polarized incident light there is a 1.5-fold reduction in the 647 cm^{-1} sapphire peak at the plasmon waveguide interface. The 647 cm^{-1} sapphire peak is completely eliminated in the PWR Raman spectrum with p-polarized incident light, and a 655 cm^{-1} analyte peak is revealed that is barely detectable in the TIR Raman spectrum. A silica background is broad across the spectral region shown in Figure 3.[18] Overall, the spectral background is lowest across the majority of the spectrum at the PWR interface, and no sign of increased silica background is measured.

Comparing the PWR Raman spectra obtained with p- and s-polarized incident light reveals that certain modes produced more scatter with p-polarized excitation when the spectra are normalized to the 1003 cm^{-1} peak. The peaks that have a higher relative intensity with p-polarized incident light are at 618, 1072, 1154, 1221, 1577, and 1595 cm^{-1}. For the peaks that are detectable, this same trend is measured in the TIR Raman spectra. The depolarization ratios and peak assignments for the pyridine modes that are enhanced with p-polarized incident light indicate that these are depolarized modes (Table 2). The differences in the Raman spectra using orthogonally polarized incident light match the published depolarization ratios for a homogeneous pyridine solution.[31] This is expected because the adsorbate, which may exhibit altered depolarization ratios, contributes no more than ~2% to the signal for a semi-infinite analyte layer.[18] The additional spectral information gained using a plasmon waveguide to enhance the Raman signal provides a means to elucidate molecular orientation of adsorbates and thin films, which may not be possible using SPR Raman spectroscopy. Another benefit is the possibility of studying a surface chemistry other than Au (i.e., SiO_2 or numerous other dielectrics).

Table 1. TIR, SPR, and PWR Raman Peak Areas for Three Analytes Collected at the Indicated Incident Angle, Which Are the Angles Where the Largest Raman Signal Was Collected at Each Interface

interface p-polarization	1.25 M pyridine measured 1003 cm^{-1} peak area (incident angle, degree)	100 nm polystyrene measured 1001 cm^{-1} peak area (incident angle, degree)	monolayer measured 995 cm^{-1} peak area (incident angle, degree)
TIR sapphire/analyte	6200 ± 300 (50.00)	1402 ± 242 (64.00)	
SPR	6800 ± 200 (52.90)		
PWR	16000 ± 300 (49.85)	5776 ± 254 (47.20)	no peak measured[a]
interface s-polarization	1.25 M pyridine measured 1003 cm^{-1} peak area (incident angle, degree)	100 nm polystyrene measured 1001 cm^{-1} peak area (incident angle, degree)	monolayer measured 995 cm^{-1} peak area (incident angle, degree)
TIR	13900 ± 200 (50.00)	2335 ± 263 (64.00)	
PWR	8400 ± 100 (51.58)	4344 ± 198 (51.89)	10131 ± 374 (50.72)[a]

[a]Average of three accumulations with a 3 min acquisition time.

dx.doi.org/10.1021/ac3013972 | Anal. Chem. 2012, 84, 9049−9055

Table 2. Raman Peak Locations and Assignments for the Indicated Analyte at the Plasmon Waveguide Interface and Depolarization Ratios Measured in Solution

pyridine peak (cm^{-1})	assignment[34] (Wilson notation)	depolarization ratio[a]
618	ν_{6a}	
1003	ν_1	0.02
1035	ν_{12}	0.01
1072	ν_{18a}	
1221	ν_{9a}	0.49
1577	ν_{8b}	0.59
1595	ν_{8a}	
polystyrene peak (cm^{-1})	**assignment[35,36]**	**depolarization ratio**
1001	ν_{12}	0.06
1034	ν_{18a}	~0
trimethyl(phenyl)silane peak (cm^{-1})	**assignment[37]**	**depolarization ratio**
995	ν_{12}	
1024	ν_{18a}	

[a]Measured in solution using a 180° backscatter geometry (i.e., not TIR).

PWR Raman Spectroscopy from a Thin Polystyrene Film. Raman spectra from a 100-nm polystyrene film at a sapphire and 49 ± 1 nm Au/548 ± 2 nm silica plasmon waveguide interface are shown in Figure 5. The spectra were collected at the incident angle where the highest signal was obtained at each interface. Similar to what was measured for the pyridine solution, one major difference between the TIR and PWR Raman spectra is the reduction in sapphire background peaks at the plasmon waveguide interface. The two polystyrene peaks that are measured at the PWR interface at 1001 and 1034 cm^{-1} have similar relative intensities using s- and p-polarized incident light, which is consist with both being polarized peaks (Table 2).

The reflected light intensity and Raman peak areas as a function of the incident angle at the plasmon waveguide interface are shown in Figure 5 for the 100-nm polystyrene film. The location of the PWR angles in the reflectivity spectra show good agreement between the calculated and experimentally measured curves for both p- and s-polarized incident light, although the amount the reflected light intensity is attenuated is calculated to be lower than what is experimentally measured. This is due to the very narrow PWR peaks compared to the instrument's angle resolution, as already discussed. The full width half-maximum of the PWR peak is 0.2° and 0.05° using p-and s-polarized incident light, respectively. The incident angle where the maximum Raman scatter is collected matches the angle where the maximum attenuation of the reflected light intensity is measured. This indicates the reflectivity curve can be used to locate the optimal incident angle for measuring Raman spectra at the PWR interface.

The MSEF extends significantly further from the interface than the 100-nm polystyrene layer at all incident angles for both the TIR and PWR interfaces. The entire film is probed at both interfaces, and a direct comparison of the Raman peak areas is possible. The Raman peak area for the 1001 cm^{-1} stretching mode is 1.9 and 4.1 times larger in the PWR spectra than in the TIR spectra for s- and p-polarized incident light, respectively (Table 2). If the instrument angle resolution was

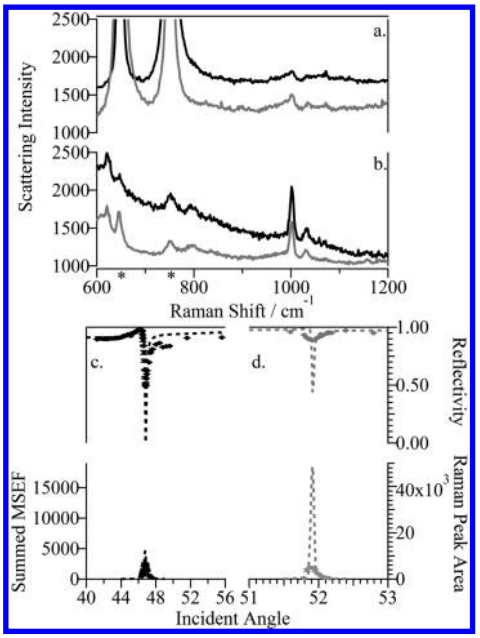

Figure 5. Raman spectra from a 100-nm polystyrene film at a (a) sapphire (TIR) interface, (b) 49 ± 1 nm Au/548 ± 2 nm SiO_2 plasmon waveguide (PWR) interface and p- (black) or s- (gray) polarized 785 nm incident light. The spectra were collected at (a) 64.00° or (b) p-polarization 47.20° and s-polarization 51.89°, which is close to the critical angle or PWR angles and where the largest Raman scatter is collected at each interface. The asterisks (*) represent peaks that are from the sapphire prism, and spectra are offset for clarity. Experimental reflectivity and Raman peak areas (symbols) from a 100-nm polystyrene film at the PWR interface with (c) p- polarized or (d) s-polarized incident 785 nm excitation. The data are fit to Fresnel reflectivity coefficients or calculated MSEF summed over the 100-nm film thickness (dotted line).

decreased to 0.01° and the incident angle spread eliminated, this could further increase the 1001 cm^{-1} peak intensity measured at the PWR interface 9.5 (s) and 1.7 (p) times.

PWR Raman Spectroscopy of a Monolayer. Monolayer detection has previously been reported for nonresonant analytes with 785 nm excitation using SPR Raman spectroscopy.[32] To assess the ability to measure a monolayer with PWR Raman spectroscopy, a monolayer of trimethyl(phenyl)silane was formed at a 49 ± 1 nm Au/630 ± 4 nm silica waveguide interface. Raman peaks were measured using s-polarized excitation near the PWR angle with a signal-to-noise ratio of 5.6 for the 995 cm^{-1} peak, but no discernible Raman signal was recorded using p-polarized excitation (Figure 6a). The calculated values shown in the Figure 2 inset (right column) correspond to the interface properties and incident angles relevant to this experiment. At the respective angles where the Raman spectra were collected, the MSEF at the interface is 10% lower for s-polarized excitation compared to p-polarized excitation. The effect of the depolarization characteristics on altering the amount of Raman scatter produced using orthogonally polarized excitation can be analyzed using TIR Raman spectroscopy with a solution of trimethyl(phenyl)silane (Figure 6b). Approximately equal 995 cm^{-1} peak intensities were recorded using p- or s-polarized light, and differences in the MSEF cannot justify the lack of Raman scatter for a trimethyl(phenyl)silane monolayer at the PWR interface using p-polarized excitation. It can be concluded that there is a uniaxial orientation of the phenyl ring relative to the substrate

dx.doi.org/10.1021/ac3013972 | Anal. Chem. 2012, 84, 9049−9055

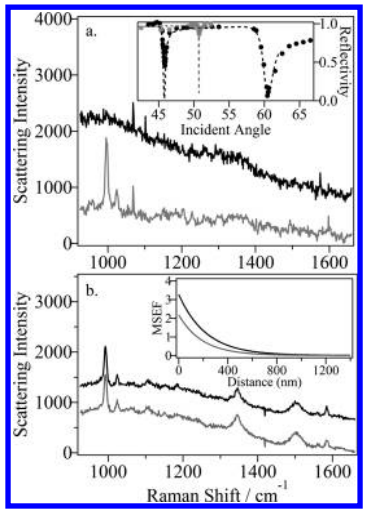

Figure 6. (a) Raman spectra from a trimethyl(phenyl)silane monolayer at a sapphire/50 ± 1 nm Au/630 ± 4 nm SiO_2 plasmon waveguide (PWR) interface and p- (black) or s- (gray) polarized 785 nm incident light. The spectra were collected at p-polarization: 45.88° and s-polarization: 50.72°, which is close to the PWR angles and where the largest Raman scatter is collected at each interface when averaging 3 accumulations with a 3 min acquisition time. The inset shows the reflected light intensity from the same interface where Raman spectra were collected. (b) Raman spectra of neat trimethyl(phenyl)silane under total internal reflection at 60.00° using a sapphire prism with a 1 min acquisition. The inset shows the relevant calculated mean square electric field as a function of distance from the interface. Spectra are offset for clarity.

at the PWR interface. This orientation could not be determined with SPR Raman spectroscopy, and low signal levels make similar TIR Raman analyses problematic. PWR Raman Spectroscopy investigations with other analytes can reveal structural details, such as tilt angles,[33] using PWR Raman spectroscopy. Further investigations are ongoing, but this is beyond the scope of the current work.

CONCLUSIONS

Previous applications of PWR spectroscopy have not provided chemically specific information, and SPR Raman spectroscopy does not allow measurements of anisotropy or chemical orientation. However, by combining PWR spectroscopy with TIR Raman spectroscopy several benefits are realized. Since the enhancement of Raman signal for analytes at the silica plasmon waveguides are not significantly higher than those measured at smooth Au films, the key benefits of using the plasmon waveguide are the ability to generate both parallel and perpendicular electric fields in the sensing layer, reduced prism backgrounds and the possibility of studying phenomena at the silica or other dielectric interfaces. The waveguides are not limited to SiO_2, and other dielectric materials are currently being explored.

AUTHOR INFORMATION

Corresponding Author

*E-mail: esmith1@iastate.edu.

Notes

The authors declare no competing financial interest.

ACKNOWLEDGMENTS

This research is supported by the U.S. Department of Energy, Office of Basic Energy Sciences, Division of Chemical Sciences, Geosciences, and Biosciences through the Ames Laboratory. The Ames Laboratory is operated for the U.S. Department of Energy by Iowa State University under Contract No. DE-AC02-07CH11358. A portion of this research was conducted at the Center for Nanophase Materials Sciences, which is sponsored at Oak Ridge National Laboratory by the Scientific User Facilities Division, Office of Basic Energy Sciences, U.S. Department of Energy. The authors thank the University of Minnesota Nanofabrication Center for assistance in fabricating plasmon waveguides and the Iowa State University Microelectronics Research Center for use of their Filmetrics instrument.

REFERENCES

(1) Ikeshoji, T.; Ono, Y.; Mizuno, T. *Appl. Opt.* **1973**, *12*, 2236−7.
(2) Hoelzer, W.; Schroeter, O.; Richter, A. *J. Mol. Struct.* **1990**, *217*, 253−64.
(3) Iwamoto, R.; Miya, M.; Ohta, K.; Mima, S. *J. Am. Chem. Soc.* **1980**, *102*, 1212−13.
(4) Iwamoto, R.; Miya, M.; Ohta, K.; Mima, S. *J. Chem. Phys.* **1981**, *74*, 4780−90.
(5) Iwamoto, R.; Ohta, K.; Miya, M.; Mima, S. *Appl. Spectrosc.* **1981**, *35*, 584.
(6) Nakanaga, T.; Takenaka, T. *J. Phys. Chem.* **1977**, *81*, 645−9.
(7) Sohn, A. F.; Tisinger, L. G.; Sommer, A. J. *Microsc. Microanal.* **2004**, *10* (Suppl2), 1316−1317.
(8) Takenaka, T.; Nakanaga, T. *J. Phys. Chem.* **1976**, *80*, 475−80.
(9) Tisinger, L. G.; Sommer, A. J. *Microsc. Microanal.* **2004**, *10*, 1318−1319.
(10) Yoshikawa, M.; Gotoh, T.; Mori, Y.; Iwamoto, M.; Ishida, H. *Appl. Phys. Lett.* **1994**, *64*, 2096−8.
(11) Woods, D. A.; Bain, C. D. *Analyst (Cambridge, United Kingdom)* **2012**, *137*, 35−48.
(12) Tyrode, E.; Rutland, M. W.; Bain, C. D. *J. Am. Chem. Soc.* **2008**, *130*, 17434−17445.
(13) Woods, D. A.; Petkov, J.; Bain, C. D. *J. Phys. Chem. B* **2011**, *115*, 7341−7352.
(14) Woods, D. A.; Petkov, J.; Bain, C. D. *J. Phys. Chem. B* **2011**, *115*, 7353−7363.
(15) Kivioja, A. O.; Jaaskelainen, A. S.; Ahtee, V.; Vuorinen, T. *Vibrational Spectroscopy* **2012**, DOI: 10.1016/j.vibspec.2012.02.014.
(16) McKee, K. J.; Smith, E. A. *Rev. Sci. Instrum.* **2010**, *81*, 043106/1−043106/6.
(17) Ishizaki, F.; Kim, M. *Jpn. J. Appl. Phys.* **2008**, *47*, 1621−1627.
(18) McKee, K. J.; Meyer, M. W.; Smith, E. A. *Anal. Chem. (Washington, DC, U. S.)* **2012**, *84*, 4300−4306.
(19) Meyer, S. A.; Le Ru, E. C.; Etchegoin, P. G. *Anal. Chem. (Washington, DC, U. S.)* **2011**, *83*, 2337−2344.
(20) Salamon, Z.; Macleod, H. M.; Tollin, G. *Biophys. J.* **1997**, *73*, 2791−2797.
(21) Hruby, V. J.; Alves, I.; Cowell, S.; Salamon, Z.; Tollin, G. *Life Sci.* **2010**, *86*, 569−574.
(22) Salamon, Z.; Brown, M. F.; Tollin, G. *Trends Biochem. Sci.* **1999**, *24*, 213−219.
(23) Salamon, Z.; Tollin, G. *Spectroscopy* **2001**, *15*, 161−175.
(24) Zhang, H.; Orosz, K. S.; Takahashi, H.; Saavedra, S. S. *Appl. Spectrosc.* **2009**, *63*, 1062−1067.
(25) Abbas, A.; Linman, M. J.; Cheng, Q. *Sens. Actuators, B* **2011**, *156*, 169.
(26) Abbas, A.; Linman, M. J.; Cheng, Q. *Biosens. Bioelectron.* **2011**, *26*, 1815.
(27) Hall, D. B.; Underhill, P.; Torkelson, J. M. *Polym. Eng. Sci.* **1998**, *38*, 2039−2045.

(28) Ay, F.; Kocabas, A.; Kocabas, C.; Aydinli, A.; Agan, S. *J. Appl. Phys.* **2004**, *96*, 7147−7153.
(29) Malitson, I. H.; Murphy, F. V., Jr; Rodney, W. S. *J. Opt. Soc. Am.* **1958**, *48*, 72−73.
(30) Boltovets, P. M.; Kravchenko, S. A.; Snopok, B. A. *Plasmonics* **2010**, *5*, 395−403.
(31) Jeanmaire, D. L.; Van Duyne, R. P. *J. Electroanal. Chem.* **1977**, *84*, 1−20.
(32) McKee, K. J.; Meyer, M. W.; Smith, E. A. *Anal. Chem. (Washington, DC, U. S.)* **2012**, *84* (10), 4300−4306, DOI: 10.1021/ac203355a.
(33) Fujiwara, K.; Watarai, H. *Langmuir* **2003**, *19*, 2658−2664.
(34) Wu, D.-Y.; Ren, B.; Jiang, Y.-X.; Xu, X.; Tian, Z.-Q. *J. Phys. Chem. A* **2002**, *106*, 9042−9052.
(35) Kellar, E. J. C.; Galiotis, C.; Andrews, E. H. *Macromolecules* **1996**, *29*, 3515−20.
(36) Loader, E. J. *J. Catal.* **1971**, *22*, 41−8.
(37) Yamakita, Y.; Isogai, Y.; Ohno, K. *J. Chem. Phys.* **2006**, *124*, 104301.